28th International Laser Radar Conference (ILRC), Bucharest, Romania, 25-29 June 2017.

Evaluation of a wavelet-based optical flow algorithm through the use of large eddy simulations

Kyle Rocha-Brownell[1,*], Pierre Dérian[2], David H. Richter[3], Peter P. Sullivan[4] and Shane D. Mayor[1]

[1]*California State University Chico, Chico, California, USA, *kyledbrownell@gmail.com*
[2]*Fluminance team, Inria Rennes - Bretagne Atlantique, Rennes, France*
[3]*The University of Notre Dame, Notre Dame, Indiana, USA*
[4]*The National Center for Atmospheric Research, Boulder, Colorado, USA*

ABSTRACT

Recent progress in observations of wind fields by scanning aerosol lidar and motion estimation algorithms elevates interest in accuracy, precision, and resolution. Toward this, we are using large eddy simulations to advect a passive tracer in the model domain to mimic atmospheric aerosol. A wavelet-based optical flow algorithm is applied to the model output in order to derive dense motion vector fields. Each motion vector is compared with the known wind velocity at the corresponding point.

1 INTRODUCTION

Lidar measurement of high-resolution, multi-component wind fields continues to pose a challenge in boundary layer and microscale meteorology. One approach, similar to that of particle image velocimetry (PIV), is to apply motion estimation algorithms to sequences of images produced by scanning elastic backscatter aerosol lidars. In recent years, significant advancement of this approach was achieved through the development of eye-safe aerosol lidars with the required performance [1, 2, 3] and new motion estimation algorithms [4, 5, 6]. However, validation of the spatial vector wind fields is still a problem since there are few other methods that can provide multi-component wind vectors at 10 m intervals over areas on the order of 10 square kilometers. Therefore, we have started using LES to test the ability of the wavelet-based motion estimation algorithm to retrieve wind fields from synthetic images that approximate what the aerosol lidar provides.

2 METHODOLOGY

Large eddy simulations are computational fluid dynamics models that resolve the largest eddies in the turbulence spectrum while parameterizing the effect of the smallest. We use the NCAR LES described in Section 2.1. We include a passive tracer in the model, which serves as a proxy for the concentration of aerosol particles. Fields of the passive tracer on horizontal cross-sections from the lowest levels of the model domain are saved in data files at time intervals of about 10 seconds to match the time between scans of a hypothetical scanning aerosol lidar. The *Typhoon* motion estimation algorithm (described in Section 2.2) reads those files and produces vector flow fields based on the motion of aerosol features. Finally, the vector motion fields are compared with the actual wind velocity fields in the model.

2.1 LES

The LES model integrates equations for a dry atmospheric planetary boundary layer under the Boussinesq approximation [7]. The model includes: a) transport equations for momentum; b) a transport equation for a conserved buoyancy variable (e.g., virtual potential temperature); c) a discrete Poisson equation for a pressure variable to enforce incompressibility; and closure expressions for subgrid-scale (SGS) variables, e.g., a subgrid-scale equation

for turbulent kinetic energy [7, 8]. An arbitrary number of passive scalars can also be accommodated. As is common practice with geophysical flows, the LES imposes rough wall boundary conditions based on a drag rule where the surface transfer coefficients are determined from Monin-Obukhov similarity functions. A high Reynolds number model for viscous dissipation is used in the closure for SGS kinetic energy, and thus molecular viscosity and diffusivity do not appear in the LES equation set. The sidewall boundary conditions are periodic and a radiation boundary condition is used at the top of the domain. The equations are integrated in time using a fractional step method. The spatial discretization is second-order finite difference in the vertical direction and pseudospectral in the horizontal planes. Dynamic time stepping utilizing a third-order Runge-Kutta scheme with a fixed Courant-Fredrichs-Lewy (CFL) number is employed. The code employs 2D MPI parallelization. Further details about the code are described by [9, 10] and references therein.

2.2 Typhoon motion estimator

Typhoon is a motion estimation software implementing a dense optical flow algorithm. It retrieves a 2D, 2-component field of apparent displacements between two images by solving a single problem. Let I_0 and I_1 be the scalar image intensity defined at discrete times t_0, t_1 and at every pixel x of the image domain Ω. The estimated displacement field u minimizes a functional of the general form:

$$J(u) = \frac{1}{2}\int_{\Omega} \left[I_0(x) - I_1(x+u(x))\right]^2 dx + \alpha f_{\text{reg}}(u)\Big\}. \quad (1)$$

The first term is known as the displaced frame difference; it connects the input image data I to the output motion u. The second term f_{reg} is the regularizer required to close the problem.This work uses the 1st-order Horn & Schunck regularizer: $f_{\text{reg}} = \frac{1}{2}\sum_{i=1,2}\int_{\Omega}|\nabla u_i|^2 dx$. This term is given more or less weight through the user-parameter α. In *Typhoon*, the motion field u is represented on multiscale wavelet bases. Such bases enable to better handle large displacements as well as accurate computations of f_{reg}. Details on the algorithm and early validations can be found in [11, 12]. More recently, *Typhoon* was successfully applied to aerosol lidar scans to retrieve horizontal wind fields [3, 5].

2.3 Experiments

Turbulence in the atmospheric boundary layer is produced by combinations of buoyancy and shear. The spatial structure of the aerosol distribution and the wind field changes dramatically as the ratio of shear to buoyant production changes. For example, when the turbulence is driven primarily by convection, a cellular organization becomes apparent in the atmospheric surface layer with broad circular areas of divergent flow separated by narrow regions of convergence and sometimes strong vertical vorticity. When the flow is driven primarily by wind shear, linear streaky structures are observed, oriented in the direction of the geostrophic flow. With both buoyancy and shear contributions, horizontal roll circulations may be observed [13]. Thus far, we have conducted 9 numerical experiments that span a wide range of buoyant and shear forcing, ranging from pure convection to neutral stratification. From each of these, comparisons of the model winds with the retrieved *Typhoon* velocity fields are performed to evaluate the algorithm's ability to capture two-component velocities across varying boundary layer structure.

3 RESULTS

For the sake of brevity, we present results from only one of the 9 experiments herein. We

chose Experiment #4 which was forced with a geostrophic wind of $10\,\mathrm{ms}^{-1}$ and a surface kinematic heat flux of $0.5\,\mathrm{Kms}^{-1}$. As a result, the aerosol and wind fields exhibit considerable cellular structure that translate downstream as they evolve rapidly. Figure 1 shows the simulated aerosol backscatter field from one of two frames that would be ingested into the *Typhoon* algorithm. Figure 2 shows the model wind speed field at the same instant in time. Figure 3 shows the wind speed field retrieved by *Typhoon*. Figure 4 shows the differences between model wind speeds and the *Typhoon* wind speed estimates. Figure 5 shows one row of the wind speeds from the model and *Typhoon*. Figures 4 and 5 show that the algorithm tends to capture the large scale wind features while missing the small scale features.

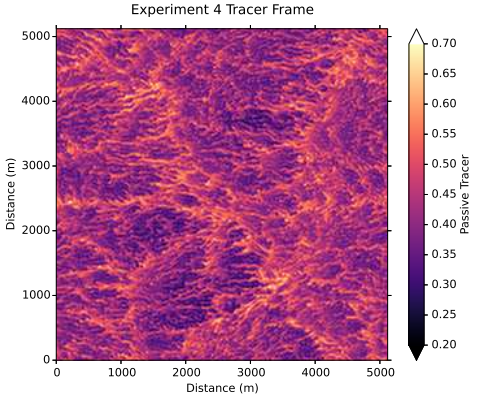

Figure 1: Passive tracer at an instant in time and from 20 m AGL from Experiment # 4.

4 CONCLUSIONS

Our hypothesis is that Typhoon would capture the large scale wind speed features and fail to resolve the small scale velocity perturbations. Our preliminary results support this hypothesis. However, to be more quantitative, we have started to calculate power spectra of the model velocity field and the *Typhoon* velocity field. The ratio of these spectra provide a transfer

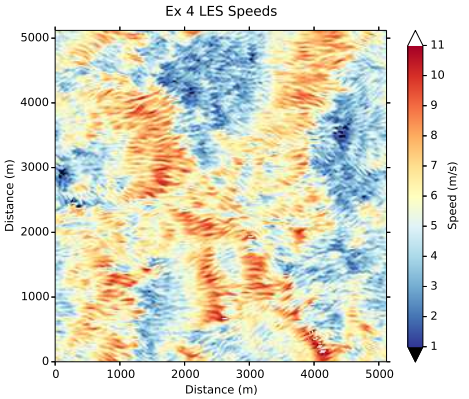

Figure 2: Model wind speed for the same instant in time as shown in Figure 1.

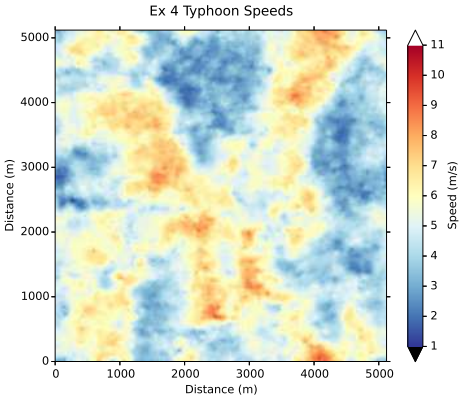

Figure 3: Wind speed as estimated by Typhoon.

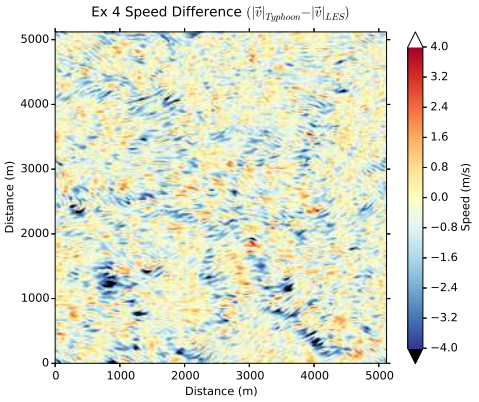

Figure 4: Differences between Typhoon and LES wind speeds.

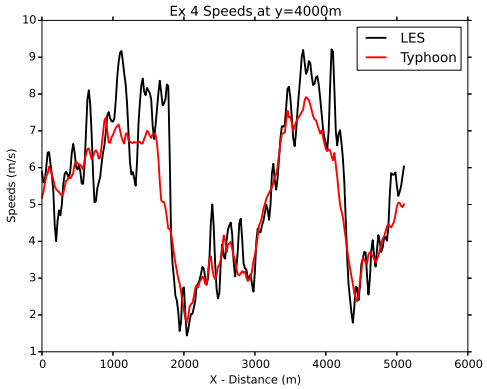

Figure 5: Typhoon and LES wind speeds for a single row of grid points at y = 4000 m.

function that shows the filtering effect and limitations of this approach to retrieve small scale wind fluctuations.

ACKNOWLEDGEMENTS

This work began under funding from NSF AGS 1228464.

References

[1] Mayor, S. D., and S. M. Spuler, 2004: Raman-shifted Eye-safe Aerosol Lidar, *Appl. Optics*, **43**, 3915- 3924.

[2] Mayor, S. D., S. M. Spuler, B. M. Morley, E. Loew, 2007: Polarization lidar at 1.54-microns and observations of plumes from aerosol generators. *Opt. Eng.*, **46**, 096201.

[3] Mayor, S. D. et al., 2016, Comparison of an analog direct detection and a micropulse aerosol lidar at 1.5-microns wavelength for wind field observations – with first results over the ocean, *J. Appl. Remote Sens.*, *10.1*, 016031.

[4] Mayor, S. D., J. P. Lowe, and C. F. Mauzey, 2012: Two-component horizontal aerosol motion vectors in the atmospheric surface layer from a cross-correlation algorithm applied to scanning elastic backscatter lidar data, *J. Atmos. Ocean. Technol.*, **29**, 1585-1602.

[5] Dérian, P., C. F. Mauzey, and S. D. Mayor, 2015: Wavelet-based optical flow for two-component wind field estimation from single aerosol lidar data. *J. Atmos. Ocean. Technol.*, **32**, 1759-1778.

[6] Hamada, M., P. Dérian, C. F. Mauzey, and S. D. Mayor, 2016: Optimization of the cross-correlation algorithm for two-component wind field estimation from single aerosol lidar data and comparison with Doppler lidar. *J. Atmos. Ocean. Technol.*, **33**, 81-101.

[7] Moeng, C-H., 1984: A large-eddy simulation model for the study of planetary boundary-layer turbulence, *J. Atmos. Sci.*, **41**, 2052-2062.

[8] Sullivan, P. P., J. C. McWilliams, and C-H. Moeng, 1994: A subgrid-scale model for large-eddy simulation of planetary boundary-layer flows, *Bound. Layer Meteor.*, **71**, 247-276.

[9] Sullivan, P. P. and E. G. Patton, 2011: The effect of mesh resolution on convective boundary-layer statistics and structures generated by large-eddy simulation, *J. Atmos. Sci.*, **68**, 2395-2415.

[10] Sullivan, P. P., J. C. Weil, E. G. Patton, H. J. J. Jonker, and D. V. Mironov, 2016: Turbulent winds and temperature fronts in large-eddy simulations of the stable atmospheric boundary layer, *J. Atmos. Sci.*, **73**, 1815-1840.

[11] Dérian, P., P. Héas, C. Herzet and E. Mémin, 2013, Wavelets and Optical Flow Motion Estimation, *Num. Math. Theor. Meth. Appl.*, **6**, 116-137.

[12] Kadri-Harouna S., P. Dérian, P. Héas, and E. Mémin, 2013, Divergence-free wavelets and high order regularization, *Int. J. Computer Vision*, **103**, 80-99.

[13] Moeng, C. and P. P. Sullivan, 1994, A comparison of shear- and buoyancy-driven planetary boundary layer flows, *J. Atmos. Sci.*, **51**, 999-1022.